Regular Article

Carrier capability of halloysite nanotubes for the intracellular delivery of antisense PNA targeting mRNA of neuroglobin gene

Andrea P. Falanga [a,1], Marina Massaro [b,1], Nicola Borbone [a,*], Monica Notarbartolo [b], Gennaro Piccialli [a], Leonarda F. Liotta [c], Rita Sanchez-Espejo [d], Cesar Viseras Iborra [d,e], Francisco M. Raymo [f], Giorgia Oliviero [g], Serena Riela [h,*]

[a] *Dipartimento di Farmacia, Università degli Studi di Napoli Federico II, Via Domenico Montesano 49, 80131 Napoli, Italy*
[b] *Dipartimento di Scienze e Tecnologie Biologiche, Chimiche e Farmaceutiche (STEBICEF), Università di Palermo, Viale delle Scienze, 90128 Palermo, Italy*
[c] *Istituto per lo Studio dei Materiali Nanostrutturati (ISMN)-CNR, Via Ugo La Malfa 153, Palermo 90146, Italy*
[d] *University of Granada, Department of Pharmacy and Pharmaceutical Technology, Faculty of Pharmacy, 18071 Granada, Spain*
[e] *Andalusian Institute of Earth Sciences, CSIC-UGR, 18100 Armilla, Granada, Spain*
[f] *Laboratory for Molecular Photonics, Department of Chemistry, University of Miami, 1301 Memorial Drive, Coral Gables 33146-0431, FL, United States*
[g] *Dipartimento di Medicina Molecolare e Biotecnologie Mediche, Via Sergio Pansini 5, 80131 Napoli, Italy*
[h] *Dipartimento di Scienze Chimiche, Viale Andrea Doria 6, 95125 Catania, Italy*

G R A P H I C A L   A B S T R A C T
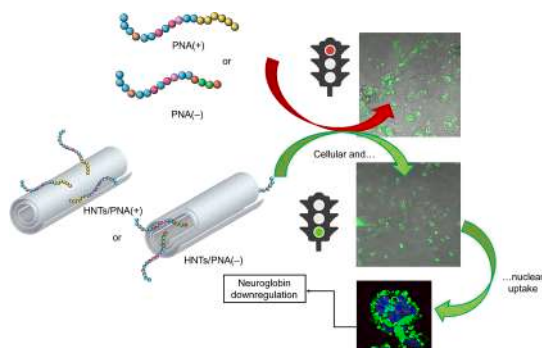
A R T I C L E   I N F O

A B S T R A C T

Peptide nucleic acid (PNA) is a DNA mimic that shows good stability against nucleases and proteases, forming strongly recognized complementary strands of DNA and RNA. However, due to its feeble ability to cross the cellular membrane, PNA activity and its targeting gene action is limited. Halloysite nanotubes (HNTs) are a natural and low-cost aluminosilicate clay. Because of their peculiar ability to cross cellular membrane, HNTs represent a valuable candidate for delivering genetic materials into cells. Herein, two differently charged 12-mer PNAs capable of recognizing as molecular target a 12-mer DNA molecule mimicking a purine-rich tract of neuroglobin were synthetized and loaded onto HNTs by electrostatic attraction interactions. After character-ization, the kinetic release was also assessed in media mimicking physiological conditions. Resonance light

* Corresponding author.
   E-mail addresses: nicola.borbone@unina.it (N. Borbone), serena.riela@unict.it (S. Riela).
[1] These authors contributed equally.

Antisense strategy
PNA

scattering measurements assessed their ability to bind complementary single-stranded DNA. Furthermore, their intracellular delivery was assessed by confocal laser scanning microscopy on living MCF-7 cells incubated with fluorescence isothiocyanate (FITC)-PNA and HNTs labeled with a probe. The nanomaterials were found to cross cellular membrane and cell nuclei efficiently.

Finally, it is worth mentioning that the HNTs/PNA can reduce the level of neuroglobin gene expression, as shown by reverse transcription-quantitative polymerase chain reaction and western blotting analysis.

1. Introduction

The design of multifunctional materials capable of performing with high selectivity and specificity multiple synergistic functions in living cells is crucial for developing smart systems for application in nano-medicine [1]. In the last few years, the peptide nucleic acid (PNA) DNA mimics have shown promising properties as gene-modulating agents. PNAs interact with complementary single-stranded DNA or RNA with higher affinity than their natural counterparts, thanks to the lower electrostatic repulsion resulting from the lack of phosphate moieties in their N-(2-aminoethyl)glycine repeating units backbone [2]. This criti-cally property, together with the low toxicity and the high chemical and enzymatic stability [3], make PNAs powerful tools in the biomedical field for the development of efficient antigene [4–6], antisense [7–9], and anti-miRNA [10–14] strategies, as well as in biosensing [15,16]. Despite these remarkable advantages, using PNAs in medical applica-tions remains a challenge because of the PNAs' poor water solubility and poor cell permeability. Accordingly, PNAs need to be delivered by car-rier systems. Over the last decades inorganic and organic nanomaterials have emerged as efficient multifunctional carrier systems for drug de-livery thanks to their unique properties, such as the nanoscale size, the high surface area, and the easily tunable surface chemistry. Conjugation of anticancer therapeutics to nanomaterials functionalized with chemi-cal moieties capable of selectively recognizing specific cancel cells will allow effective and targeted delivery of PNAs into tumor tissues [17,18]. In addition, the implementing of rationally designed functionalization strategies, which exploit the physical encapsulation and/or chemical conjugation of different drugs to the same nanocarrier, allows the development of multidrug-releasing platforms that improve the efficacy of treatments [19]. In this context, clay minerals, phyllosilicates with nanometric dimensions used in healthcare since ancient times due to their intrinsic properties, are among the most promising [20]. Among them, halloysite ($Al_2Si_2O_5(OH)_4 \cdot nH_2O$), an aluminosilicate clay mineral belonging to the kaolin group, holds great potential as a drug carrier because of its peculiar tubular nanostructure (usually referred to as halloysite nanotubes, HNTs).

Compared to other nanomaterials, HNTs are natural, available in large amounts at low cost, and, thanks to the empty lumen (Ø 15 nm), can be used for loading hydrophobic molecules ensuring their slow and sustained release [21,22]. HNTs consist of rolled kaolinite sheets, where siloxane groups are localized at the external surface, and the aluminum hydroxide ones are exposed in the lumen. Consequently, the HNTs' outer surface is negatively charged, whereas the inner lumen is positive [23]. The opposite charges localization significantly influences the ag-gregation and dispersion of HNTs in aqueous media and opens the way to the differential functionalization of the external surface and lumen. Different studies assessed the biocompatibility of HNTs [24] and proved that HNTs penetrate the external cellular membrane and accumulate in the perinuclear area [25–27]. This ability allows the transport and release even high molecular weight potential drugs into the cytoplasm [28].

In a recent work, halloysite nanotubes were used as carriers to enhance the solubility of a PNA model strand and allow its delivery into breast cancer (MCF-7) and multidrug-resistant acute myeloid leukemia (HL60-R) human cancer cell lines [29]. The fluorescently labeled 4mer TCGA PNA sequence was covalently attached to the external halloysite surface through a pH-sensitive imine bond, and its cellular uptake was

assessed by confocal laser-scanning microscopy. The analysis of the CLSM images confirmed that HNTs could efficiently transport the PNA cargo inside the cells near the perinuclear region. More recently, su-pramolecular interactions between differently charged PNA tetramers and HNTs highlighted selective surface modification depending on the PNA tetramer's charge, influencing their kinetic release in media mimicking physiological conditions [30].

Herein, to translate the positive results of the proof-of-concept study regarding interactions of differently charged PNA tetramers with HNTs [30], two different 12-mer PNA molecules, bearing polylysine (PNA(+)) or a two serine-phosphate (PNA(–)) tail (Table 1), were synthesized to achieve a selective functionalization of the outer or inner surface of HNTs, respectively (Fig. 1), using electrostatic interactions. The 12-mer-PNA molecules possess nucleobase sequence capable of recognizing as molecular target a 12-mer DNA molecule mimicking a purine-rich tract of neuroglobin (NGB) mRNA as assayed by using electrophoretic (PAGE) and spectroscopic techniques (circular dichroism (CD) and CD melting). It is reported that NGB protein is upregulated in glioma [31], breast [32], and non-small cell lung cancer tissues [33] compared to healthy tissues; thus, the inhibition of its expression by using an antisense pyrimidine-rich 12-mer PNA complementary to the selected tract of the NGB mRNA could represent a real-world scenario to assess the poten-tialities of the proposed HNTs-based PNA delivery system.

After the PNA(+) and PNA(–) molecules synthesis and character-ization, they were loaded onto HNTs surfaces and the successful func-tionalization was verified by Fourier-transform infrared spectroscopy (FT-IR) and thermogravimetric analysis (TGA). The aqueous mobility upon functionalization was studied by dynamic light scattering (DLS) measurement and the overall charge by ζ-potential investigations. The morphology of the nanomaterials was investigated by transmission electron microscopy (TEM). Once verified the selective surfaces func-tionalization, both PNAs were simultaneously loaded onto HNTs (HNTs/PNA(–)/PNA(+)). To evaluate the PNA release performances of the obtained complexes, the kinetic release of the PNA molecules from HNTs/PNA(–), HNTs/PNA(+) and HNTs/PNA(–)/PNA(+) nano-materials was investigated by dialysis bag method in media mimicking physiological conditions. Furthermore, the ability of HNTs/PNA nano-materials to bind complementary single stranded DNA was assessed by resonance light scattering (RLS) measurements choosing HNTs/PNA(+) as model.

To study the capability of the HNTs based nanocarriers to deliver their PNA cargo into cells, cell uptake studies were performed by confocal laser scanning microscopy (CLSM) on MCF-7 cells incubated with HNTs functionalized with fluorescein isothiocyanate (FITC)-labelled PNA(+) and PNA(–). Furthermore, to verify the nuclear uptake of both components of the developed nanomaterials (HNTs and PNAs),

Table 1
Sequences of PNAs used in this study.

Sample	Sequence
PNA(+)	H_2N-cccacctctgcc-(lys)$_6$-CONH$_2$
FITC-PNA(+)	FITC-(AEEA)$_2$-cccacctctgcc-(lys)$_6$-CONH$_2$
PNA(–)	H_2N-cccacctctgcc-gly-ser(P)-ser(P)-gly-CONH$_2$
FITC-PNA(–)	FITC-(AEEA)$_2$-cccacctctgcc-gly-ser(P)-ser(P)-gly –CONH$_2$
DNA1	d5´-GGCAGAGGTGGG-3´
DNA2	d5´-CCCACCTCTGCC –3´

PNA bases in lowercase letters.

these were labeled with a fluorescent probe (**1Cl**) [27] and the cell nuclei were stained with 4′,6-diamidino-2-phenylindole (DAPI).

Finally, to evaluate the ability of HNTs/PNAs to recognize a cellular target, therefore validating the intracellular and nuclear uptake of the synthetized nanomaterials, MCF-7 cells were incubated in the presence of PNA(+), HNTs or HNTs/PNA(+) and the reduction of the level of neuroglobin gene expression was evaluated by reverse transcription-quantitative polymerase chain reaction (RT-qPCR) and western blotting analysis.

2. Results and discussion

2.1. Design and synthesis of DNA and PNA molecules

We used publicly available bioinformatic tools to select the nucleobase sequence for the synthesis of a PNA molecule capable of down-regulating the NGB expression at the translational level. At first, we visually inspected the mature NGB mRNA (NCBI Reference Sequence: NM_021257.4) searching for purine-rich 12-nucleotides-long short sequences to be targeted by a pyrimidine-rich complementary antisense PNA because of the higher synthetic yield achievable for the synthesis of PNA strands having a high pyrimidines content (https://www.pnabio.com/support/PNA_Tool.htm). Then, using the OligoAnalyzer™ Tool (https://eu.idtdna.com) we chose among the selected candidates the 12-mer GGCAGAGGTGGG sequence whose complementary PNA strand was predicted to be less prone to fold into ordered secondary structures or self-dimers. Accordingly, using the solid phase strategy described in the

Experimental Section we synthesized the PNA(+) and PNA(−) molecules (Table 1) bearing a six lysins or a two serine phosphate tail at their carboxamide end to allow the electrostatic interaction with the outer and inner surfaces of HNTs, respectively. We also synthesized the FITC labelled FITC-PNA(+) and FITC-PNA(−) to monitor the delivery and cellular localization of the PNA cargo by HNTs in MCF-7 cells using CLSM.

Considering that the stability of PNA-RNA duplexes is higher than those of corresponding PNA-DNA analogs [34] and the higher resistance towards nucleases of DNA strands compared to the corresponding RNA strands, we synthesized the 12-mer DNA analog of the target mRNA sequence (DNA1, Table 1) to assess the hybridization of PNA(+) and PNA(−) with the complementary DNA target model (PNA/DNA 1:1 ratio) using PAGE, CD, and CD melting analyses.

The molecular size of the complexes formed by incubating FITC-PNA (+) with DNA1 was examined by PAGE analysis in 100 mM PBS (Fig. 2) using the migration rate of DNA1, its complementary DNA strand DNA2, and that of the DNA1/DNA2 duplex as controls. The gel was visualized by UV irradiation at 260 nm and 365 nm, and by Sybr Green staining (transilluminator at 260 nm) to reveal the DNA, the FITC labelled PNA, and the DNA ladder, respectively. The annealed DNA1/DNA2 mixture migrated as one single band having a mobility similar to the 10 bp DNA ladder, in agreement with the expected mobility of the 12-mer DNA duplex model (lane 1A, Fig. 2). The gel runs of DNA1 and DNA2 (lanes 2 and 3, respectively, Fig. 2A) were characterized by the presence of a strong band having a mobility within the 5–10 bp DNA ladder range due to the random coil DNA strands. The second pale band observed in lane
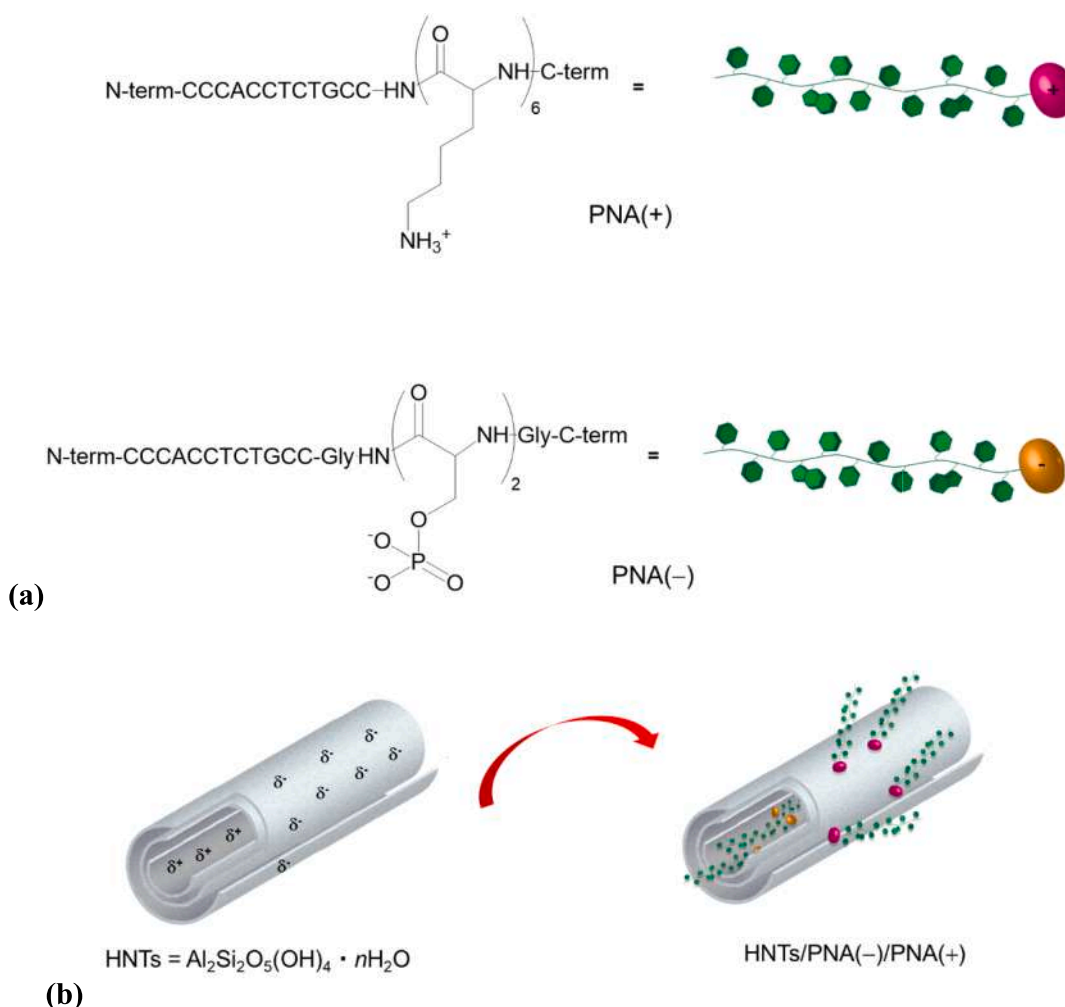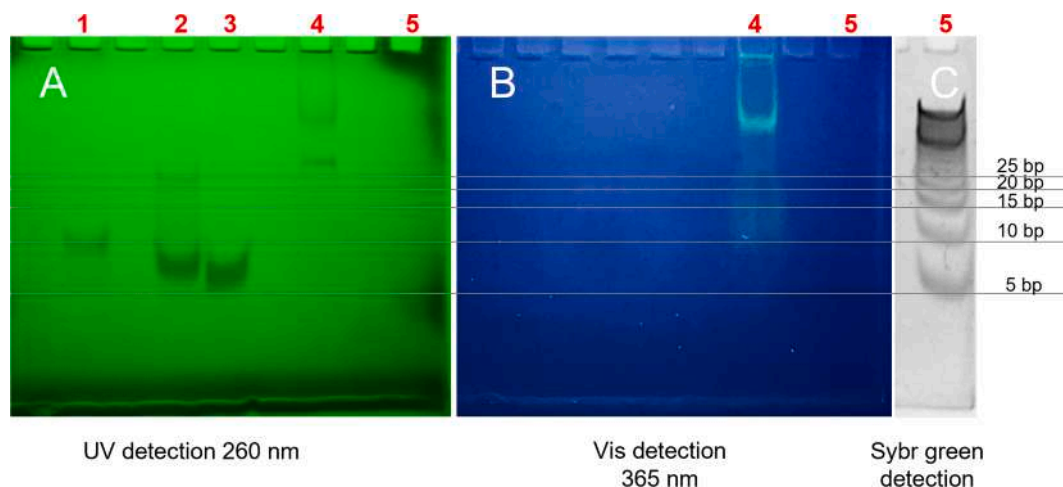

Fig. 1. Structure of the synthesized (a)12-mer-PNA molecules and (b) HNTs based nanomaterial.

Fig. 2. PAGE revealed at 260 nm (A), 365 nm (B) using an UV–Vis lamp and after Sybr Green staining at 260 nm using a Biorad transilluminator (C). Lane 1A: DNA1/DNA2 mixture 1:1; lane 2A: DNA1 alone; lane 3A: DNA2 alone; lanes 4A and 4B: FITC-PNA(+)/DNA1; lanes 5: DNA ladder. All samples were annealed at 1 mM concentration in the presence of PBS 100 mM buffer, pH 7.4.

2A revealed that DNA1 formed a small amount of higher molecular weight aggregates. The migration pattern of the FITC-PNA(+)/DNA1 1:1 mixture was characterized by the disappearance of the band ascribable to the single strand DNA1 and the presence of two new more retained bands. We attributed the faster band to high molecular weight aggregates of DNA1, and the second most retarded band to the FITC-PNA(+)/DNA1 heteroduplex. This hypothesis was strengthened by the FITC-induced yellowish color observed for this band under 365 nm UV lamp irradiation (lane 4B, Fig. 1). A small amount of the not migrating unbound FITC-PNA(+) was observed on the bottom of well 4 because of its positive charge and the absence of interaction with the negatively charged DNA1.

To further confirm the formation of the PNA(+)/DNA1 heteroduplex and estimate its thermal stability we performed CD and CD melting analyses in comparison with the corresponding DNA duplex (Fig. 3A). The CD spectrum of DNA1/DNA2 mixture (solid line) showed the typical spectrum of an antiparallel DNA duplex, with two positive bands at 204 and 268 nm and a negative band at 238 nm [35]. The CD profile of PNA(+)/DNA1 sample (dashed line) was in agreement with those reported for antiparallel PNA/DNA heteroduplexes [36], featuring two CD maxima at 221 and 266 nm and one minimum at 243 nm, thus confirming the formation of the PNA/DNA heteroduplex. Moreover, we observed a significant increase in the intensity of the positive dichroic signal at 266 nm for PNA(+)/DNA1 relative to DNA1/DNA2 profile. This evidence can be ascribed to the higher affinity of PNA strands for the complementary RNA and DNA strands due to the absence of charges in the PNA backbone that reduces the electrostatic repulsion between the two molecules. The CD melting curve reported in Fig. 2B allowed us to estimate the apparent melting temperature of the PNA(+)/DNA1 heteroduplex in near physiological condition. The calculated value of 68 °C resulted to be considerably higher than those estimated for the corresponding DNA/DNA and RNA/DNA analogues (respectively equal to 52.6 and 55.3 °C according to the prediction given by the OligoAnalyzer™ Tool) and significantly higher than the physiological body temperature.

2.2. Synthesis of HNTs/PNA nanomaterials

The loading of PNA(+) and PNA(–) into halloysite nanotubes was carried out by mixing a dispersion of halloysite in CHCl$_3$ (25 mg mL^{-1})

C	Λ min (nm)	Λ max (nm)
duplex	238	204-268
heteroduplex	243	221-266
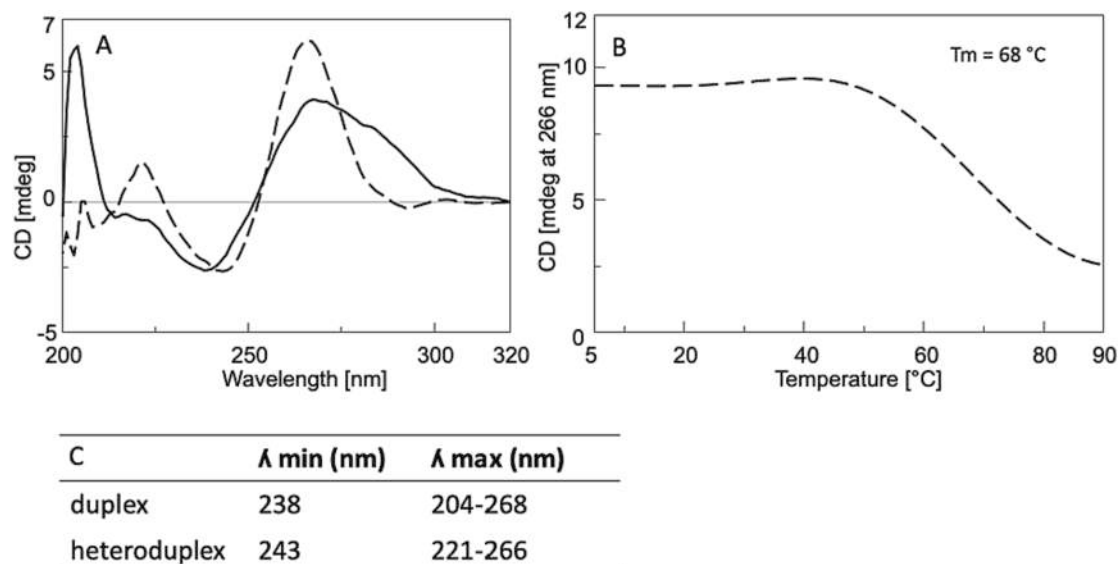
Fig. 3. (A) CD profiles of DNA1/DNA2 (solid line) and PNA(+)/DNA1 (dashed line). The samples were annealed at the 20 µM single strand concentration in 100 mM PBS buffer, pH 7.4. (B) CD melting curve of PNA(+)/DNA1 recorded at 266 nm. (C) Table of CD minima and maxima.

with 0.5 mL of 2 mg mL^{-1} aqueous solution of PNA(+) or PNA(−). For samples incubated with PNA(−), the fresh dispersions were evacuated for 3–5 min to promote the loading of the molecule into the HNTs lumen and left to stir at room temperature for 18 h. After work-up, the amounts of PNA loaded into HNTs were determined by thermogravimetric analyses (TGA) as of ca. 1.2 wt% and 1.3 wt% for HNTs/PNA(−) and HNTs/PNA(+), respectively (Scheme 1).

The HNTs/PNA nanomaterials were characterized by FT-IR spectroscopy and TGA, and the colloidal properties were estimated by DLS and ζ-potential measurements. Furthermore, the morphology of the nanomaterials was imaged by TEM and high-angle annular dark field scanning transmission electron microscopy (HAADF-STEM).

In Fig. 4a are reported the FT-IR spectra of the HNTs/PNA(−) and HNTs/PNA(+) nanomaterials and for comparison the FT-IR spectrum of pristine HNTs. As it is possible to observe, the HNTs spectrum shows two bands at 3622 and 3693 cm^{-1} corresponding to the O—H stretching of the inner hydroxyl groups and outer surface hydroxyl groups, respectively [37]. Additionally, a broad signal at 1640 cm^{-1} is attributed to the H—O—H bending of H-bonded water on the halloysite structure, which corresponds to the broad O—H stretching signal at 3550 cm^{-1}. Apical Si—O and Si—O—Si stretching vibrations provided the bands at 1115 and 1031 cm^{-1}, respectively. The bands at 753 and 690 cm^{-1} derive from the perpendicular Si—O stretching vibration. The O—H deformation vibration of inner Al—O—H groups generates the band at 912 cm^{-1}. Beside these typical bands, the FT-IR spectra of both nanomaterials show additional vibration bands, such as the bands at ca. 2900 and 2850 cm^{-1} which arise from the stretching vibration of methylene groups and some bands in the range 1600–1400 cm^{-1} attributable to the stretching of C=N and C=C groups of the organic molecules loaded into the HNTs lumen.

Fig. 4b shows the TGA curve of HNTs/PNA(−), HNTs/PNA(+) and that of pristine HNTs. All present the typical mass loss of halloysite, due to expulsion of the interlayer water molecules of HNTs. By comparing the TGA curves of HNTs/PNA(−) and HNTs/PNA(+) nanomaterials with that of the pristine HNTs, a slight mass loss between ∼ 240–290 °C is observed for both samples, a bit more pronounced for HNTs/PNA(−). Such mass loss was attributed to the removal of the PNA currently to the elimination of some residual water molecules adsorbed onto halloysite surface of the samples. By increasing the temperature, the mass continued gradually to decrease up to the massive weight loss in the range between 450 and 520 °C due to removal of the interlayer water molecules typical of HNTs structure. According to TG analyses, on the basis of the final mass value achieved at 900 °C, the loading of PNA was estimated to be ca. 1.2 wt% and 1.3 wt% for HNTs/PNA(−) and HNTs/PNA(+), respectively.

The structural characteristics of the HNTs/PNA(−) and HNTs/PNA(+) nanomaterials were investigated by monitoring their mobility in water through DLS measurements. By this technique, indeed, it was possible to calculate the average translational diffusion coefficient, which is related to the dimension and shape of the diffusing particles, their hydration, solvent viscosity, and aggregation phenomena. HNTs are anisotropic objects with a high aspect ratio, which can change due to functionalization. Moreover, particles ability to interact and aggregate can also depend on surface decoration. Thus, a detailed quantitative analysis of the results was hampered. Valuable information was achieved by using the Stokes-Einstein equation to calculate the average diameter of the equivalent sphere, which can be considered as an index to follow the changes in particle dimensions and interparticle aggregation. In this study, the Z-average size of the particles in dispersion were of ca. 480 nm and 1900 nm for HNTs/PNA(−) and HNTs/PNA(+), respectively. These results agree with the selective functionalization of HNTs surface, indeed in the case of HNTs/PNA(−), the value of the Z-average size agrees with the negatively charged PNA loading into HNTs lumen, being the average size of pristine HNTs of ca. 500 nm. Conversely, the high value of Z-average size obtained in the case of HNTs/PNA(+) is indicative with the functionalization of the external HNTs surface by the positively charged PNA(+), and what we observed was a collective motion of nanoparticles keep together by the supramolecular association among the different PNA units.

ζ-potential measurements showed that the HNTs/PNA(−) nanomaterial presents a negative charge (−21.8 ± 0.8 mV), more negative in comparison to the ζ-potential of pristine halloysite (−16 mV) further confirming the partial neutralization of the positive charge at the inner surface after PNA(−) loading. On the contrary, the ζ-potential value of HNTs/PNA(+) was ca. −14.0 ± 0.9 mV in agreement with the functionalization of the HNTs external surface. These results were in agreement with literature data, reporting the use of halloysite as carrier for similar molecules [30].

The morphology of the different nanomaterials was imaged by TEM and high-angle annular dark field scanning transmission electron microscopy (HAADF-STEM). The TEM image of the two HNTs/PNA nanomaterials (Fig. 5A and Fig. 6A) showed that structure of the HNTs nanomaterial was preserved after PNA loading. Both nanomaterials indeed exhibited the characteristic hollow tubular structure of halloysite with some differences. In comparison to the HNTs/PNA(−) nanomaterial (Fig. 5A), the TEM images of HNTs/PNA(+) nanomaterial showed a compact structure indicating the existence of some attraction interactions among the PNA molecules present at the HNTs external surface (Fig. 6A).

Energy-dispersive X-ray spectroscopy (EDS) elemental mapping
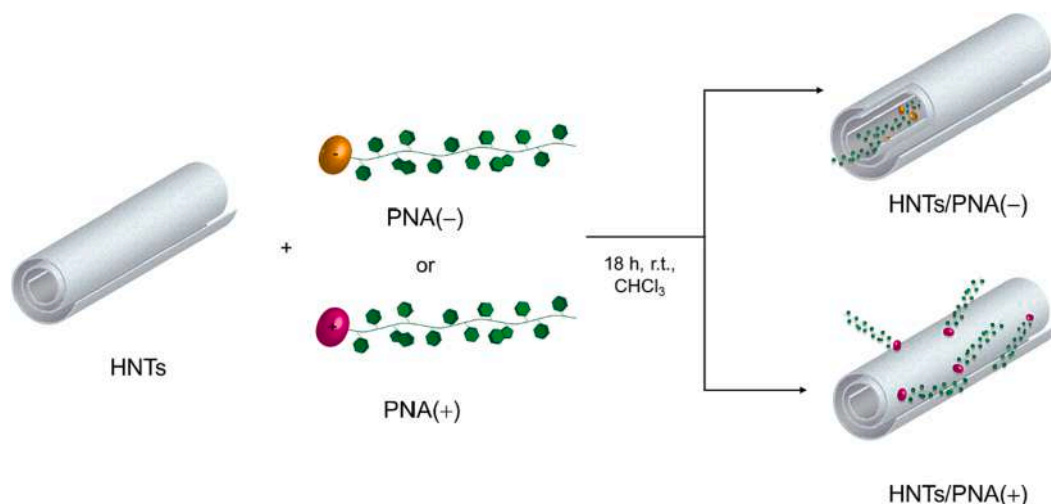
Scheme 1. Schematic representation of HNTs/PNA(−) and HNTs/PNA(+) nanomaterials.
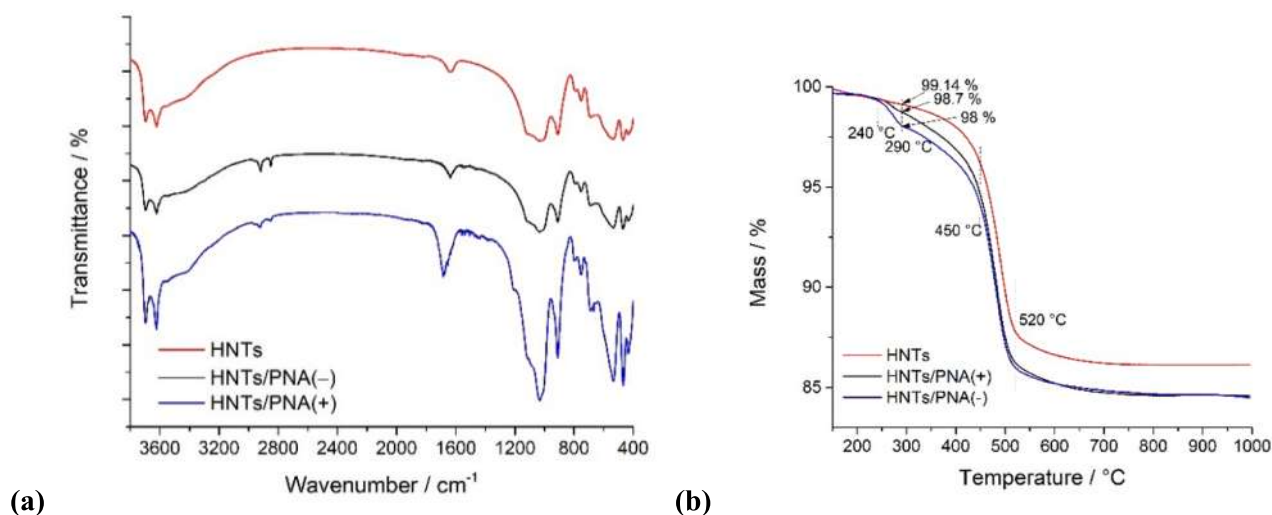
Fig. 4. (a) FT-IR spectra and (b) thermogravimetric curves of HNTs, HNTs/PNA(+) and HNTs/PNA(−) nanomaterials.
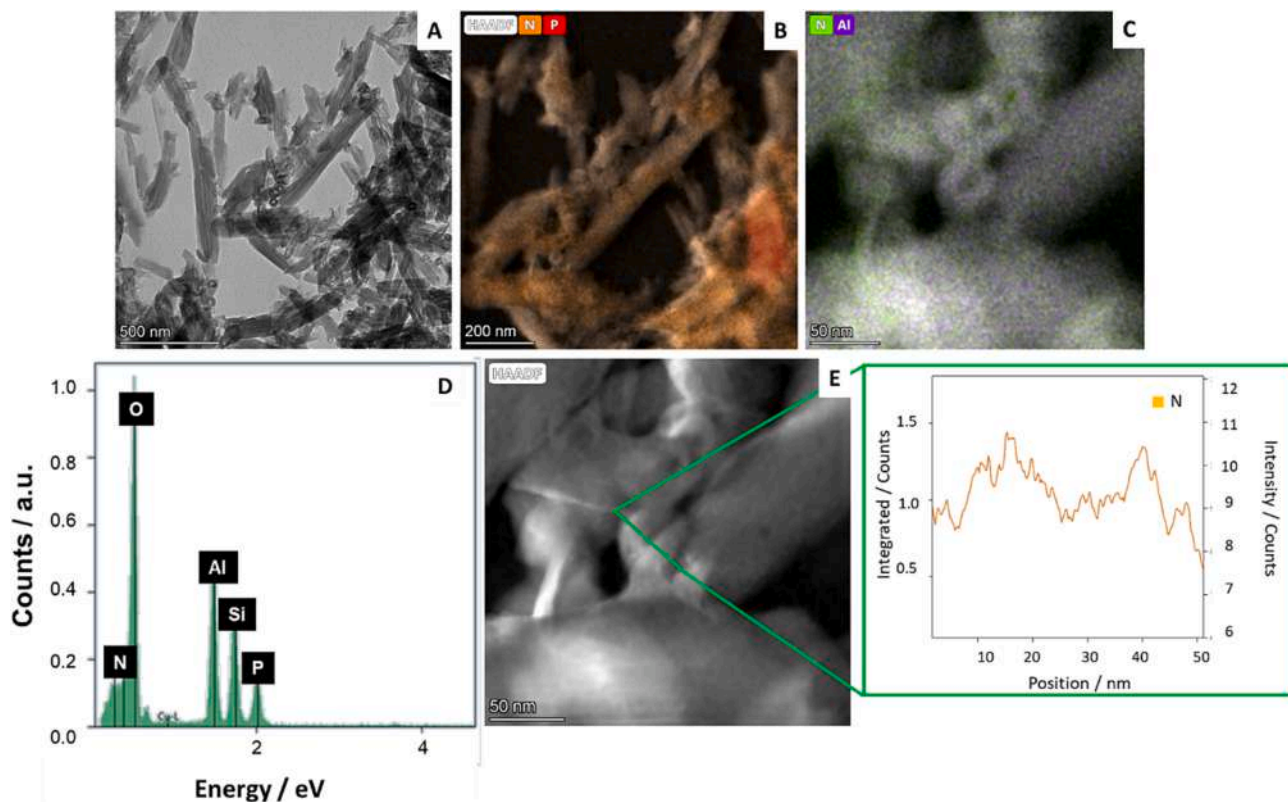

Fig. 5. (A) TEM of the HNTs/PNA(−) nanomaterial. (B-C) EDX elemental mapping images. (D) EDS analysis and (E) EDS elemental mapping of N atoms along the selected area of the HAADF-STEM image of the HNTs/PNA(−) nanomaterial.

showed that the PNA molecules were present on the overall surface of the tubes, as highlighted by the distribution of N atoms (highlighted in orange in all samples) and P atoms in the case of PNA(−) molecules (Fig. 4B-D and Fig. 5B-D). Moreover, close observation of the tubes showed the presence of N atoms mainly localized in proximity of HNTs lumen in the case of nanomaterial HNTs/PNA(−) (Fig. 5E), whereas they are mainly localized at the external surface of HNTs in the HNTs/PNA (+) nanomaterial as proven by EDS elemental mapping performed along the HNTs section (Fig. 6E).

Once confirmed that the selective modification of HNTs surfaces occurs depending on the different charge of the PNA molecules, the

double modification of HNTs was performed. Therefore, the PNA(−) loading into HNTs was carried out by vacuum cycling of a HNTs suspension in a saturated PNA(−) solution. This cycle was repeated several times to obtain the highest loading efficiency. After loading, the HNTs/PNA(−) nanomaterial was recovered and suspended again in $CHCl_3$ and then to this dispersion an aqueous solution of PNA(+) was added. Finally, the double modified HNTs/PNA(−)/PNA(+) nanomaterial was recovered and subjected to further investigations (Scheme 2).

The aqueous dispersion of the HNTs/PNA(−)/PNA(+) showed a Z-average size value of ca. 1900 nm in agreement with the external surface functionalization and a ζ-potential value of ca. $−13.7 \pm 0.8$ mV further
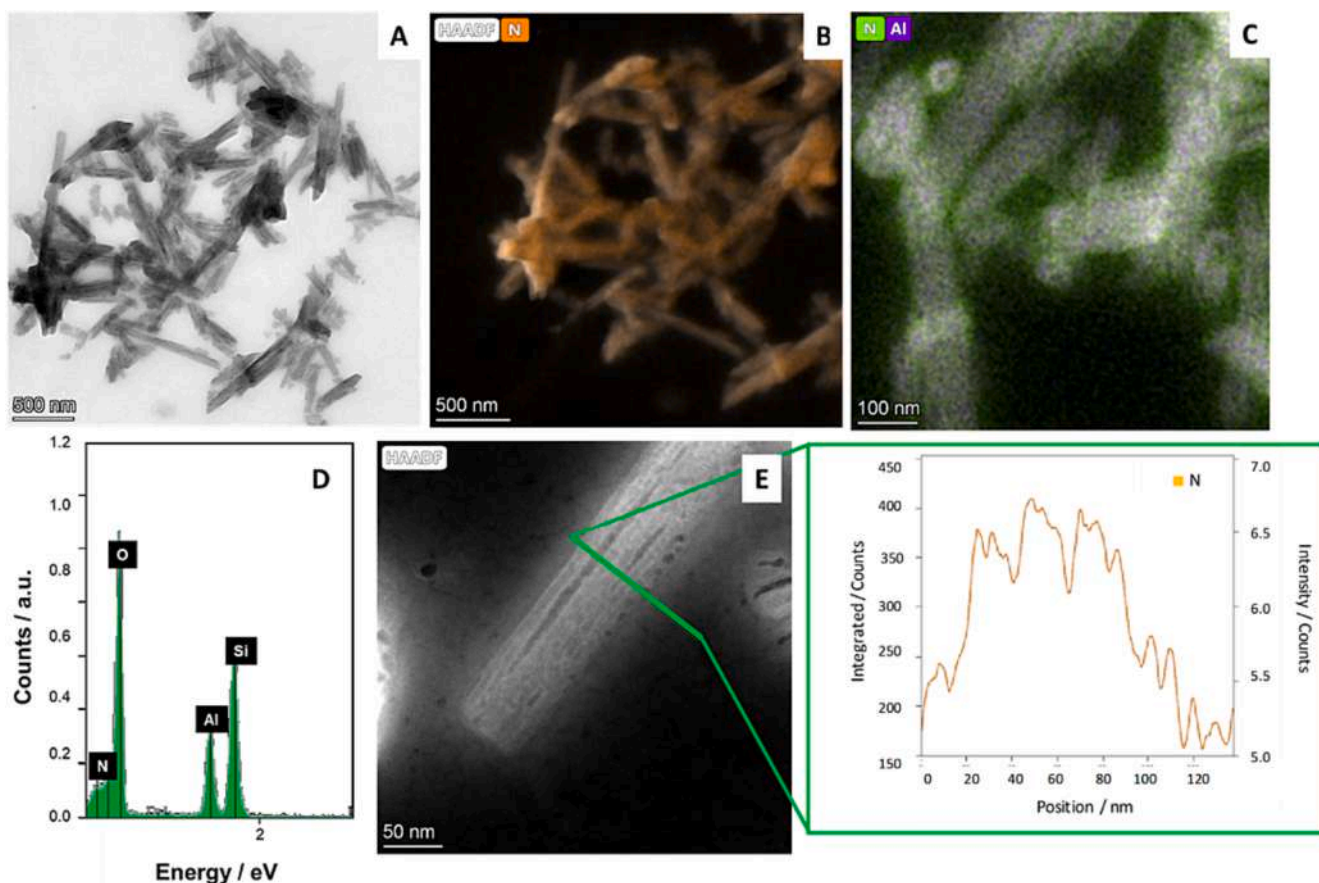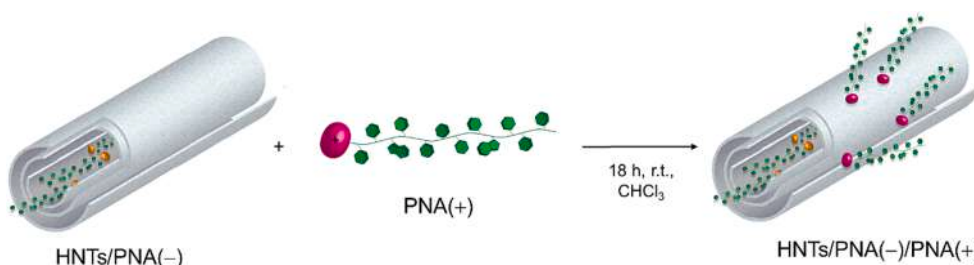
Fig. 6. (A) TEM of the HNTs/PNA(+) nanomaterial. (B-C) EDX elemental mapping images. (D) EDS analysis and (E) EDS elemental mapping of N atoms along the selected area of the HAADF-STEM image of the HNTs/PNA(+) nanomaterial.

Scheme 2. Schematic representation of the synthesis of the double modified HNTs/PNA(–)/PNA(+) nanomaterial.

confirms the successful modification.

2.3. Kinetic release

To evaluate the performances of the obtained nanomaterials for application in biomedical field, the kinetic release of the different PNA molecules from HNTs/PNA(–), HNTs/PNA(+) and HNTs/PNA(–)/PNA(+) nanomaterials was evaluated by the dialysis bag method at pH 7.0 to mimic physiological conditions. The obtained kinetic data are reported in Fig. 7. As it is possible to observe, the HNTs/PNA(–) nanomaterial showed a fast release in the first 100 min where ca. 40 wt% of the total amount of PNA loaded is released, reaching the total amount released after 24 h. This release profile is coherent with the loading of molecules inside the HNTs lumen which benefit of slow and sustained release within time. On the contrary, the release of PNA molecules from HNTs/PNA(+) nanomaterial was very fast reaching the 100 wt% of molecules released after ca. 300 min. This behavior agrees with the desorption of

molecules from the HNTs external surfaces. A similar release profile was obtained in the case of the HNTs/PNAs nanomaterial. Also, in this case the total amount of PNA loaded was released in ca. 350 min.

The kinetic data were analyzed by different mathematical models to obtain information about the release mode. Three different models, namely first-order, Power Fit, and the double exponential model (DEM) were applied. The obtained fits revealed that the release of PNA molecules from HNTs/PNA(–) follows the first order model ($k = 0.0028 \pm 0.0003$ min^{-1}, $R^2 = 0.9911$) indicating a diffusion from the HNTs lumen; similar results were obtained for the PNA release from HNTs/PNA(+) ($k = 0.045 \pm 0.005$ min^{-1}, $R^2 = 0.9904$). Conversely, the PNA release from the HNTs/PNAs nanomaterial is better described by DEM ($R^2 = 0.9984$). Since DEM describes the release mode of two spectroscopically distinguishable species, in this case we observed a fast release of the PNA molecules interacting with the HNTs external surface ($k = 0.14 \pm 0.01$ min^{-1}) and at the same time, a slower diffusion of the molecules from the HNTs lumen ($k = 0.0040 \pm 0.0008$ min^{-1}).
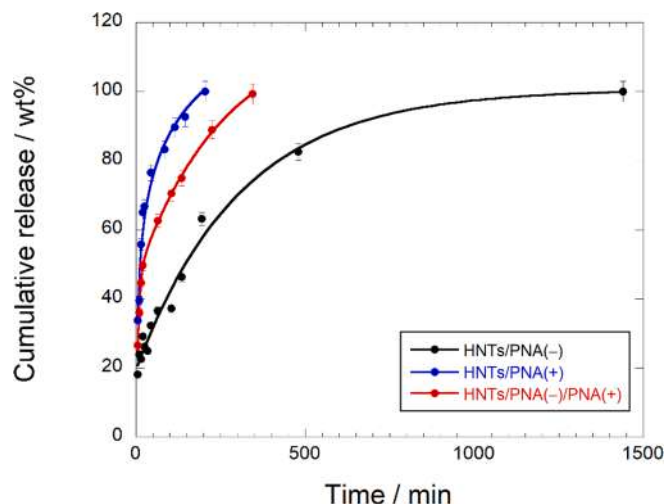
Fig. 7. Kinetic release of PNA molecules from HNTs/PNA(–), HNTs/PNA(+), and HNTs/PNA(–)/PNA(+) nanomaterials at pH 7.0 and 37 °C averaged over two independent experiments.

2.4. Study of the interaction between the HNTs/PNA(+) nanomaterials and the complementary DNA

To verify if the PNA molecules loaded onto HNTs retained their ability to bind complementary DNAs some studies by Resonance Light Scattering (RLS) measurements were performed. This technique, based on the fluctuations of the solution refraction index, gives information about the presence of aggregates in solution and therefore it can be used for the determination of aggregation phenomena between molecules and nanomaterials. RLS experiments were performed by keeping HNTs/PNA(+), chosen as model, concentration constant (0.002 mg mL^{-1}) and titrating with an increasing concentration of complementary ssDNA in the concentration range 0–15 μg mL^{-1} at 25 °C. In Fig. 8 the trend of RLS intensity at 540 nm as function of DNA concentration is reported. As it is possible to observe the RLS intensity increases by increasing the amount of DNA added, reaching a plateau at a concentration of DNA of ca. 3 μg mL^{-1} which corresponds to a stoichiometric ratio PNA/DNA of 1:1.
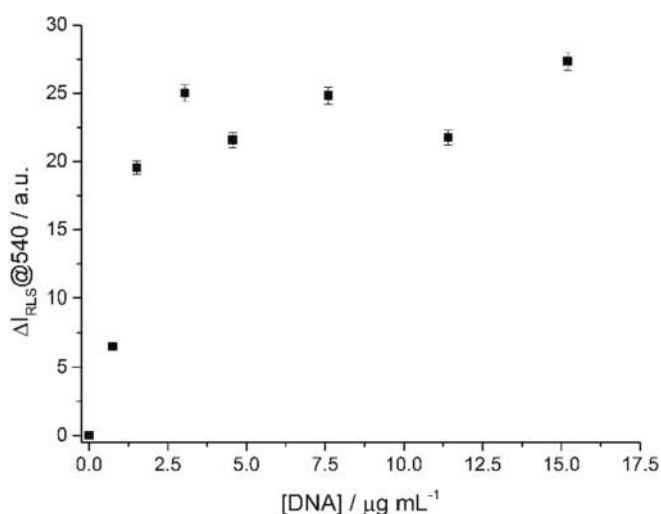

Fig. 8. Trend of RLS intensity at 540 nm of HNTs/PNA(+) nanomaterial (0.002 mg mL^{-1}) as a function of complementary DNA (ranging from 0 to 15 μg mL^{-1}), averaged over two independent experiments.

2.5. Cellular uptake

To study the capability of the HNTs carrier to deliver PNA molecules into cells, uptake studies were performed by CLSM using FITC-PNA(+) and FITC-PNA(–) which were obtained as described in the Experimental Section.

The obtained FITC-PNA molecules (+and –) were loaded onto HNTs following the same procedure described above, obtaining fluorescent nanomaterials with a loading of PNA of ca. 1 wt% in both cases, namely HNTs/FITC-PNA(–) and HNTs/FITC-PNA(+), as estimated by TGA (see SI). As reported in Figure S14, the thermogravimetric curves exhibit the same behavior up to 500 °C, suggesting that in the range between 100 and 500 °C the removal of the same species occurs for the two samples. Then, above 500 °C, the HNTs/FITC-PNA(+) starts to lose further weight up to reaching the residual mass value of 84.8 % at 900 °C. The HNTs/FITC-PNA(–) giving the same curve as HNTs up to 650 °C, above such temperature degraded up to the final value of 84.8 % at 900 °C, as for the (+) peptide.

The cellular uptake of the obtained nanomaterial was investigated by CLSM experiments. HNTs/FITC-PNA(–) and HNTs/FITC-PNA(+) nanomaterials and for comparison FITC-PNA(–) and FITC-PNA(+) molecules (10 mM) were incubated on MCF-7 (breast cancer) living cell lines, at different time (3, 6 and 24 h). It was observed that after 3 h of incubation, both FITC-PNA molecules did not penetrate cellular membranes, as proved by the green fluorescence localized outside cells (Figure S15A-C), in agreement with the low cellular permeability showed by this kind of molecules [38]. On the contrary, the HNTs/FITC-PNA(–) and HNTs/FITC-PNA(+) nanomaterials were efficiently uptaken by the cells, as proved by the green spots localized in the perinuclear region (Figure S15D-F).

Higher incubation time (6 h) highlighted that the nanomaterials are able to penetrate nuclear membrane, as demonstrated by Z-stacking experiments, imaging the three-dimensional shape of cells at various focal planes (data not shown). To further prove this finding, cell lines incubated for 24 h with the synthetized nanomaterials were washed, fixed, and stained with DAPI (diamidino-2-phenylindole), a blue fluorescent probe that shows a bright emission when bind the minor groove of double stranded DNA. As it is possible to observe from confocal images (Fig. 9A-C), PNA(+) did not penetrate cellular membrane as shown by the absence of green fluorescence related to FITC-PNA inside cells (Fig. 9A). On the contrary, the co-localization of the blue fluorescence related to DAPI and the green one associated with both HNTs/PNAs nanomaterials, confirms the presence of the latter inside the cells with cytoplasmic and nuclear localization (Fig. 9B-C), in particular it infers that PNA molecules could bind cellular DNA at the level of nucleoli. Furthermore, close observations showed that in the cell treated with HNTs-PNAs nanomaterials, incomplete DAPI staining occurs probably because of a pairing of the PNA molecules with their complementary DNA.

From a qualitative analysis HNTs/PNA(–) shows a lower nuclear uptake than HNTs/PNA(+) (Fig. 9D-E); this finding could be explained on the basis of the different interacting HNTs surface with the differently charged 12-mer-PNA molecules. HNTs/PNA(–), indeed, showed the presence of PNA(–) molecules into clay lumen, thus they are slowly released in physiological conditions (Fig. 9E); conversely HNTs/PNA(+) nanomaterial shows the PNA(+) at the HNTs external surface, more available to fast penetrate in the nuclear region (Fig. 9D). Enhanced cellular and nuclear uptake of halloysite-based nanomaterials was indeed detected when the HNTs external surface was modified with suitable molecules, such as carbon dots [39] or targeting molecules as biotin or folic acid [40–42].

Finally, to further verify that the green fluorescence observed inside cells is not only due to the FITC-PNA molecules but also to the HNTs/PNA nanomaterial, the systems were also labelled with a fluorescent coumarin chromophore combined with a switchable halochromic oxazine (**1Cl**) that was shown to interact strongly with HNTs (Fig. 9F) [27].
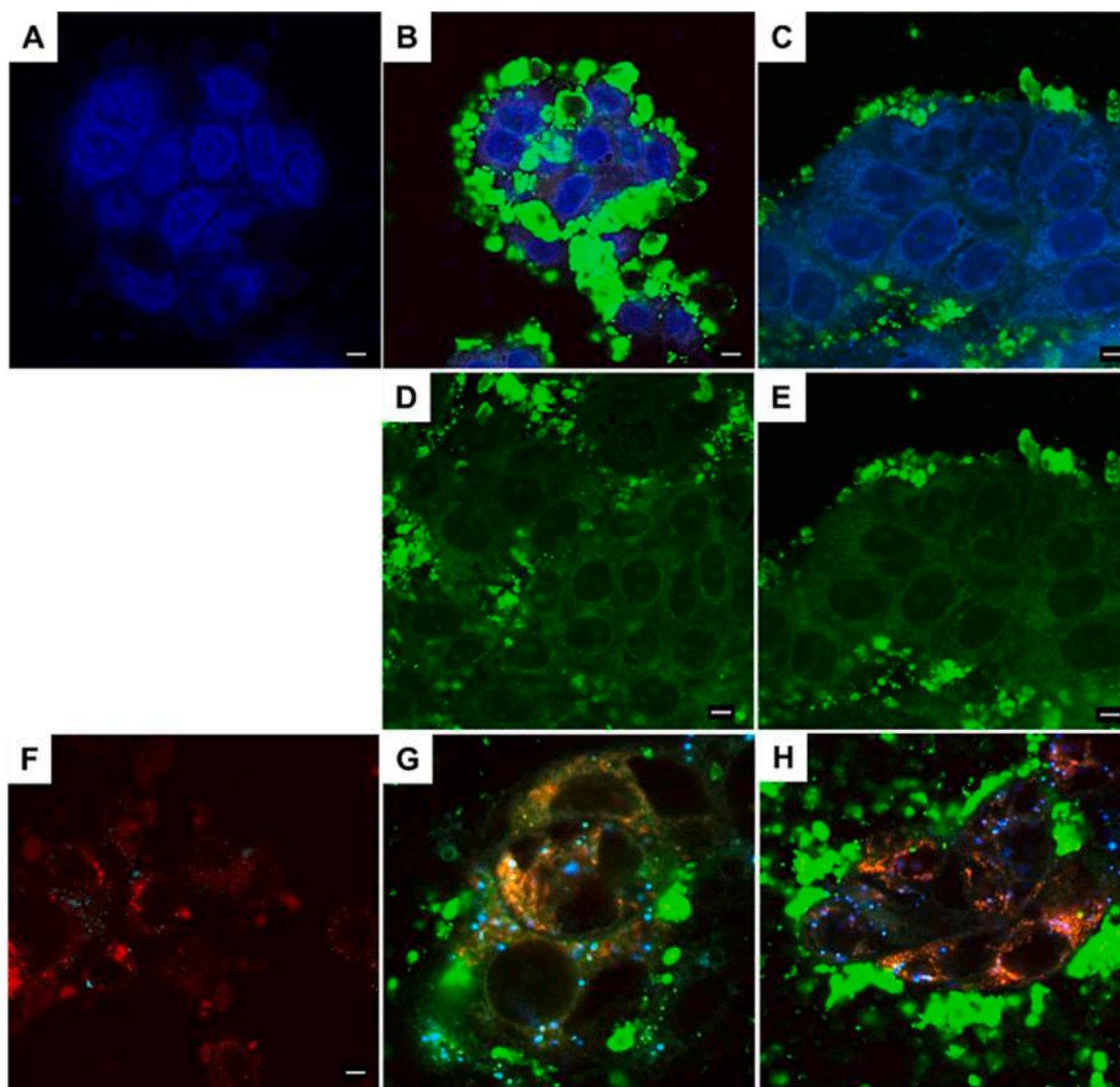
Fig. 9. Merged CLSM images of MCF-7 cells incubated for 24 h with (A) FITC-PNA(+); (B-D) HNTs/FITC-PNA(+), (C-E) HNTs/FITC-PNA(–) fixed and stained with DAPI; (F) HNTs/**1Cl**; (G) HNTs/FITC-PNA(+)/**1Cl** and (H) HNTs/FITC-PNA(–)/**1Cl**. Scale bar: 50 μm, magnification 60×.

1Cl molecule has the peculiarity of emitting in different region of the electromagnetic spectrum in response to pH. As it is possible to observe, the co-existence of the three colors in the same cellular region (Fig. 9G-H), proves that all components of the HNTs/PNA nanomaterials (HNTs, **1Cl**, and PNA-FITC) penetrate into cells and thus, HNTs can represent a valuable carrier for the delivery of genetic material.

2.6. Inhibition of the neuroglobin expression mediated by HNTs/PNA

To evaluate the ability of HNTs/PNAs to recognize a cellular target, therefore validating the intracellular and nuclear uptake of the synthetized nanomaterials, MCF-7 cells were incubated in the presence of PNA (+), HNTs or HNTs/PNA(+) (10 μM), chosen as models, for 24 h and the reduction of the level of neuroglobin gene expression was evaluated by reverse transcription-quantitative PCR (RT-qPCR). No inhibition of the protein expression was observed after treatment with HNTs and PNA(+) molecules(Fig. 10), the latter further indicate that PNA(+) alone cannot penetrate cellular membrane as already observed by CLSM investigations. Conversely, a clear reduction in neuroglobin expression was observed in the cells incubated with HNTs/PNA(+).

Thus, the levels of the neuroglobin protein through western blotting

analysis (Fig. 11) after 48 h of exposure to the HNTs/PNA(+) nanomaterial at the same concentrations used in the gene expression assays, was also evaluated. These results indicate that the loading of PNA(+) on HNTs improves its uptake and intracellular delivery in MCF-7 cells and drives targeted neuroglobin silencing.

The cell viability assays showed that HNTs/PNA(+) treatment was not toxic to the cells up to 100 μM concentration.

3. Conclusions

The design of innovative nanosystems for the delivery of genetic material inside cells is a challenge for nanomedicine. Peptide nucleic acid (PNA) DNA mimics have shown promising properties as gene-modulating agents, but their clinical use if often limited, since they show a very low cellular uptake and, due to this currently only one PNA, among the different synthetized ones, is in clinical trials as drug [43]. Finding new carrier systems which can overcome this limitation is thus crucial. In the last years some inorganic systems, such as zeolite and silica, have been considered as carrier system for the delivery of PNA, and recently, the use of halloysite, a natural, biocompatible, and low-cost clay mineral resulted very promising for biotechnological
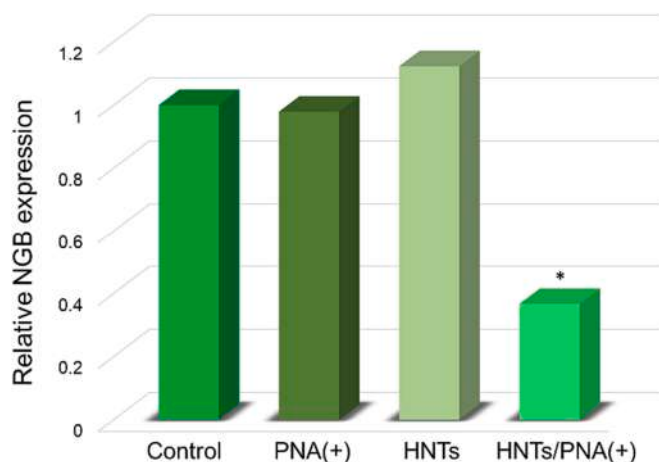
Fig. 10. Evaluation of target mRNA expression levels in MCF-7 cell lines. For each condition, N = 3 technical replicates were used. Data are expressed as mean ± standard error of three experiments (Figure S5). Differences when treatments are compared to the control, *p < 0.01 (one-way ANOVA followed by Tukey's test).

applications. The use of halloysite for the delivery of specific PNA molecules designed to selectively recognize a molecular target is not reported so far.

In the present work, different HNTs based nanomaterials were developed for the intracellular delivery of antisense PNA molecules targeting the mature mRNA of neuroglobin gene. Two different 12-mer-PNA molecules, bearing positive and negative tails were *ad hoc* synthetized to achieve a selective HNTs surfaces' modification by mean of electrostatic interaction with either the external HNTs' surface or the internal lumen, respectively.

Afterwards, the two 12-mer-PNA molecules were supramolecularly loaded onto HNTs and the obtained nanomaterials were thoroughly characterized by several techniques. FT-IR spectroscopy and TGA allowed us to confirm the presence of the PNA molecules onto HNTs, whereas by DLS and ζ-potential measurements it was confirmed the selectivity in the interaction. The HNTs/PNA(–) nanomaterial indeed showed a translational diffusion close to that of pristine HNTs and a ζ-potential value more negative than that of HNTs in agreement with PNA(–) lumen confinement. On the contrary, the HNTs/PNA(+) nanomaterial showed a slower diffusion mode in aqueous dispersion and ζ-potential value slightly more positive than that of HNTs confirming the

PNA(+) interaction with HNTs external surface.

Morphological investigations highlighted that the HNTs/PNA(+) nanomaterial showed a compact structure where the molecule is present at the clay external surface, as showed by the N elemental mapping extrapolated by EDS measurements. Once verified the selective surfaces functionalization, both PNAs were simultaneously loaded onto HNTs (HNTs/PNA(–)/PNA(+)) and the kinetic release of the different nanomaterials was investigated by dialysis bag method in media mimicking physiological conditions. It was found that the PNA release is strictly correlated to the interaction surface onto HNTs. The PNA(+) molecules were indeed totally released from HNTs/PNA(+) nanomaterial in ca. 350 min, whereas the release of PNA(–) from HNTs/PNA(–) nanomaterial is sustained over the time reaching the total release after 24 h. The release of PNA from the HNTs/PNA(–)/PNA(+) nanomaterial was found to be a combination of the two-release mode.

The HNTs/PNA(+) nanomaterial, chosen as model, showed that the PNA molecule retains the ability to recognize complementary DNA as verified by RLS.

The increase of cellular uptake of PNAs after their loading onto HNTs was verified by CLSM investigations on MCF-7 cell lines. Conversely to PNA molecules, the HNTs/PNAs nanomaterials penetrate the cellular membrane even after 3 h. After 24 h of incubation, the HNTs/PNAs nanomaterials were localized into cytoplasmatic area and in the nuclear region as confirmed by the nanomaterials labelling with a fluorescent probe and nuclei DAPI staining.

The neuroglobin expression inhibition experiments prove the feasibility of the HNTs/PNA nanomaterials synthetized for future applications, opening the use of HNTs as delivery systems for gene silencing therapy. Indeed, these experiments confirm that PNA molecules cannot be internalized into cells, whereas the HNTs/PNA nanomaterials can penetrate inside them, localizing into cytoplasmatic region, and depending on PNA nucleobase sequence, they can be uptaken also inside cell nuclei where they can recognize the complementary nucleobase sequence silencing the gene expression.

The reported study represents a step forward to the use of HNTs as delivery system for PNA molecules and is promising for future applications in gene therapy. In light of the non-biodegradability of halloysite, it is possible to hypothesize a future use of the developed systems for oral, topical, or local administration, for the treatment as example of solid tumors. Future works will be focused on the development of fluorescent carriers based on halloysite for the simultaneous co-delivery of PNAs and other therapeutic agents.
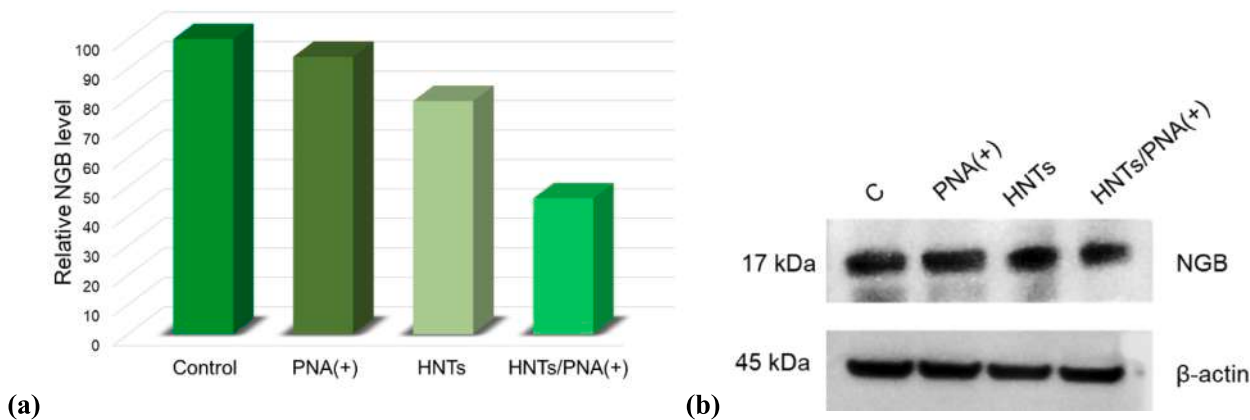
Fig. 11. Western blotting analysis of the neuroglobin level in MCF-7 cells, (a) results expressed as relative protein level (mean ± standard error of two different experiments, Figure S6); β-actin was used as loading control. *HNT/PNA vs C *P* < 0.01 (one-way ANOVA followed by Tukey's test); (b) results of a representative experiment. Irrelevant parts of the gel image (such as blank lanes and lanes with molecular weight markers) are deleted. The samples were derived from the same experiment and gels/blots were processed in parallel.

CRediT authorship contribution statement

Andrea P. Falanga: Formal analysis, Investigation, Methodology, Writing – original draft, Writing – review & editing. **Marina Massaro:** Formal analysis, Investigation, Methodology, Writing – original draft, Writing – review & editing. **Nicola Borbone:** Conceptualization, Formal analysis, Supervision, Writing – original draft, Writing – review & editing. **Monica Notarbartolo:** Conceptualization, Investigation, Methodology, Writing – original draft, Writing – review & editing. **Gennaro Piccialli:** Data curation, Methodology, Resources. **Leonarda F. Liotta:** Investigation, Methodology, Writing – original draft. **Rita Sanchez-Espejo:** Investigation, Methodology, Writing – original draft. **Cesar Viseras Iborra:** Data curation, Methodology, Resources. **Francisco M. Raymo:** Data curation, Methodology, Resources. **Giorgia Oliviero:** Conceptualization, Investigation, Methodology, Writing – original draft, Writing – review & editing. **Serena Riela:** Conceptualization, Formal analysis, Supervision, Writing – original draft, Writing – review & editing.

Declaration of competing interest

The authors declare that they have no known competing financial interests or personal relationships that could have appeared to influence the work reported in this paper.

Data availability

Data will be made available on request.

Acknowledgements

Appendix A. Supplementary material

Supplementary data to this article can be found online at https://doi.org/10.1016/j.jcis.2024.02.136.

References

[1] Z. Su, S. Dong, S.-C. Zhao, K. Liu, Y. Tan, X. Jiang, Y.G. Assaraf, B. Qin, Z.-S. Chen, C. Zou, Novel nanomedicines to overcome cancer multidrug resistance, Drug Resist. Updat. 58 (2021) 100777.

[2] E. Uhlmann, A. Peyman, G. Breipohl, D.W. Will, PNA: Synthetic Polyamide Nucleic Acids with Unusual Binding Properties, Angew. Chem. Int. Ed. 37 (20) (1998) 2796–2823.

[3] M. Pooga, T. Land, T. Bartfai, Ü. Langel, PNA oligomers as tools for specific modulation of gene expression, Biomol. Eng 17 (6) (2001) 183–192.

[4] J. Amato, B. Pagano, N. Borbone, G. Oliviero, V. Gabelica, E.D. Pauw, S. D'Errico, V. Piccialli, M. Varra, C. Giancola, G. Piccialli, L. Mayol, Targeting G-Quadruplex Structure in the Human c-Kit Promoter with Short PNA Sequences, Bioconjug. Chem. 22 (4) (2011) 654–663.

[5] J. Amato, M.I. Stellato, E. Pizzo, L. Petraccone, G. Oliviero, N. Borbone, G. Piccialli, A. Orecchia, B. Bellei, D. Castiglia, C. Giancola, PNA as a potential modulator of COL7A1 gene expression in dominant dystrophic epidermolysis bullosa: a physico-chemical study, Mol. Biosyst. 9 (12) (2013) 3166–3174.

[6] A.P. Falanga, V. Cerullo, M. Marzano, S. Feola, G. Oliviero, G. Piccialli, N. Borbone, Peptide Nucleic Acid-Functionalized Adenoviral Vectors Targeting G-Quadruplexes in the P1 Promoter of Bcl-2 Proto-Oncogene: A New Tool for Gene Modulation in Anticancer Therapy, Bioconjug. Chem. 30 (3) (2019) 572–582.

[7] C.G. Janson, M.J. During, Peptide Nucleic Acids, Morpholinos and Related Antisense Biomolecules, 1 ed., Springer, New York, 2014.

[8] E. Cesaro, A.P. Falanga, R. Catapano, F. Greco, S. Romano, N. Borbone, A. Pastore, M. Marzano, F. Chiurazzi, S. D'Errico, G. Piccialli, G. Oliviero, P. Costanzo, M. Grosso, Exploring a peptide nucleic acid-based antisense approach for CD5 targeting in chronic lymphocytic leukemia, PLoS One 17 (3) (2022).

[9] M. Terracciano, F. Fontana, A.P. Falanga, S. D'Errico, G. Torrieri, F. Greco, C. Tramontano, I. Rea, G. Piccialli, L. De Stefano, H.A. Santos, N. Borbone, Development of Surface Chemical Strategies for Synthesizing Redox-Responsive Diatomite Nanoparticles as a Green Platform for On-Demand Intracellular Release of an Antisense Peptide Nucleic Acid Anticancer Agent, Small 18 (41) (2022).

[10] F. Amato, R. Tomaiuolo, N. Borbone, A. Elce, J. Amato, S. D'Errico, G. De Rosa, L. Mayol, G. Piccialli, G. Oliviero, G. Castaldo, Design, synthesis and biochemical investigation, by in vitro luciferase reporter system, of peptide nucleic acids as new inhibitors of miR-509-3p involved in the regulation of cystic fibrosis disease-gene expression, MedChemComm 5 (1) (2014) 68–71.

[11] F. Amato, R. Tomaiuolo, F. Nici, N. Borbone, A. Elce, B. Catalanotti, S. D'Errico, C. M. Morgillo, G. De Rosa, L. Mayol, G. Piccialli, G. Oliviero, G. Castaldo, Exploitation of a Very Small Peptide Nucleic Acid as a New Inhibitor of miR-509-3p Involved in the Regulation of Cystic Fibrosis Disease-Gene Expression, Biomed Res. Int. 2014 (2014) 610718.

[12] F. Zarrilli, F. Amato, C.M. Morgillo, B. Pinto, G. Santarpia, N. Borbone, S. D'Errico, B. Catalanotti, G. Piccialli, G. Castaldo, G. Oliviero, Peptide Nucleic Acids as miRNA Target Protectors for the Treatment of Cystic Fibrosis, Molecules 22 (7) (2017) 1144.

[13] E. Fabbri, A. Tamanini, T. Jakova, J. Gasparello, A. Manicardi, R. Corradini, A. Finotti, M. Borgatti, I. Lampronti, S. Munari, M.C. Dechecchi, G. Cabrini, R. Gambari, Treatment of human airway epithelial Calu-3 cells with a peptide-nucleic acid (PNA) targeting the microRNA miR-101-3p is associated with increased expression of the cystic fibrosis Transmembrane Conductance Regulator (CFTCR) gene, Eur. J. Med. Chem. 209 (2021) 112876.

[14] M. Comegna, G. Conte, A.P. Falanga, M. Marzano, G. Cernera, A.M. Di Lullo, F. Amato, N. Borbone, S. D'Errico, F. Ungaro, I. d'Angelo, G. Oliviero, G. Castaldo, Assisting PNA transport through cystic fibrosis human airway epithelia with biodegradable hybrid lipid-polymer nanoparticles, Sci. Rep. 11 (1) (2021) 6393.

[15] R. Moretta, M. Terracciano, N. Borbone, G. Oliviero, C. Schiattarella, G. Piccialli, A. P. Falanga, M. Marzano, P. Dardano, L. De Stefano, I. Rea, PNA-Based Graphene Oxide/Porous Silicon Hybrid Biosensor: Towards a Label-Free Optical Assay for Brugada Syndrome, Nanomaterials 10 (11) (2020) 2233.

[16] T. Crisci, A.P. Falanga, M. Casalino, N. Borbone, M. Terracciano, G. Chianese, M. Gioffrè, S. D'Errico, M. Marzano, I. Rea, L. De Stefano, G. Oliviero, Bioconjugation of a PNA Probe to Zinc Oxide Nanowires for Label-Free Sensing, Nanomaterials 11 (2) (2021) 523.

[17] N. Barkalina, C. Charalambous, C. Jones, K. Coward, Nanotechnology in reproductive medicine: Emerging applications of nanomaterials, Nanomedicine: Nanotechnology, Biol. Med. 10 (5) (2014) e921–e938.

[18] A. Wicki, D. Witzigmann, V. Balasubramanian, J. Huwyler, Nanomedicine in cancer therapy: Challenges, opportunities, and clinical applications, J. Control. Release 200 (2015) 138–157.

[19] S. Ghosh, R. Lalani, V. Patel, D. Bardoliwala, K. Maiti, S. Banerjee, S. Bhowmick, A. Misra, Combinatorial nanocarriers against drug resistance in hematological cancers: Opportunities and emerging strategies, J. Control. Release 296 (2019) 114–139.

[20] D. Peixoto, I. Pereira, M. Pereira-Silva, F. Veiga, M.R. Hamblin, Y. Lvov, M. Liu, A. C. Paiva-Santos, Emerging role of nanoclays in cancer research, diagnosis, and therapy, Coord. Chem. Rev. 440 (2021).

[21] S. Sepahi, M. Kalaee, S. Mazinani, M. Abdouss, S.M. Hosseini, Introducing electrospun polylactic acid incorporating etched halloysite nanotubes as a new nanofibrous web for controlled release of Amoxicillin, J. Nanostruct. Chem. 11 (2) (2021) 245–258.

[22] L. Lisuzzo, G. Cavallaro, S. Milioto, G. Lazzara, Halloysite nanotubes filled with salicylic acid and sodium diclofenac: effects of vacuum pumping on loading and release properties, J. Nanostruct. Chem. 11 (4) (2021) 663–673.

[23] C. Bretti, S. Cataldo, A. Gianguzza, G. Lando, G. Lazzara, A. Pettignano, S. Sammartano, Thermodynamics of Proton Binding of Halloysite Nanotubes, J. Phys. Chem. C 120 (14) (2016) 7849–7859.

[24] M.V. Gorbachevskii, A.V. Stavitskaya, A.A. Novikov, R.F. Fakhrullin, E.V. Rozhina, E.A. Naumenko, V.A. Vinokurov, Fluorescent gold nanoclusters stabilized on halloysite nanotubes: in vitro study on cytotoxicity, Appl. Clay Sci. 207 (2021).

[25] Y. Lvov, A. Aerov, R. Fakhrullin, Clay nanotube encapsulation for functional biocomposites, Adv. Colloid Interface Sci. 207 (2014) 189–198.

[26] S. Riela, A. Barattucci, D. Barreca, S. Campagna, G. Cavallaro, G. Lazzara, M. Massaro, G. Pizzolanti, T.M.G. Salerno, P. Bonaccorsi, F. Puntoriero, Boosting the properties of a fluorescent dye by encapsulation into halloysite nanotubes, Dyes Pigm. 187 (2021).

[27] M. Massaro, M. Notarbartolo, F.M. Raymo, G. Cavallaro, G. Lazzara, M.M. A. Mazza, C. Viseras-Iborra, S. Riela, Supramolecular Association of Halochromic Switches and Halloysite Nanotubes in Fluorescent Nanoprobes for Tumor Detection, ACS Appl. Nano Mater. (2022).

[28] M. Massaro, G. Cavallaro, C.G. Colletti, G. D'Azzo, S. Guernelli, G. Lazzara, S. Pieraccini, S. Riela, Halloysite nanotubes for efficient loading, stabilization and controlled release of insulin, J. Colloid Interface Sci. 524 (2018) 156–164.

[29] M. Massaro, E. Licandro, S. Cauteruccio, G. Lazzara, L.F. Liotta, M. Notarbartolo, F. M. Raymo, R. Sánchez-Espejo, C. Viseras-Iborra, S. Riela, Nanocarrier based on halloysite and fluorescent probe for intracellular delivery of peptide nucleic acids, J. Colloid Interface Sci. 620 (2022) 221–233.

[30] S. Riela, A. Borrego-Sánchez, S. Cauteruccio, R. de Melo Barbosa, M. Massaro, C. I. Sainz-Díaz, R. Sánchez-Espejo, C. Viseras-Iborra, E. Licandro, Exploiting the interaction between halloysite and charged PNAs for their controlled release, J. Mater. Chem. B (2023).

[31] J. Hu, X. Cao, D. Pang, Q. Luo, Y. Zou, B. Feng, L. Li, Z. Chen, C. Huang, Tumor grade related expression of neuroglobin is negatively regulated by PPARγ and confers antioxidant activity in glioma progression, Redox Biol. 12 (2017) 682–689.

[32] M. Fiocchetti, M. Cipolletti, S. Leone, A. Naldini, F. Carraro, D. Giordano, C. Verde, P. Ascenzi, M. Marino, Neuroglobin in Breast Cancer Cells: Effect of Hypoxia and Oxidative Stress on Protein Level, Localization, and Anti-Apoptotic Function, PLoS One 11 (5) (2016) e0154959.

[33] U. Oleksiewicz, N. Daskoulidou, T. Liloglou, K. Tasopoulou, J. Bryan, J.R. Gosney, J.K. Field, G. Xinarianos, Neuroglobin and myoglobin in non-small cell lung cancer: Expression, regulation and prognosis, Lung Cancer 74 (3) (2011) 411–418.

[34] K.K. Jensen, H. Ørum, P.E. Nielsen, B. Nordén, Kinetics for Hybridization of Peptide Nucleic Acids (PNA) with DNA and RNA Studied with the BIAcore Technique, Biochemistry 36 (16) (1997) 5072–5077.

[35] M. Vorlíčková, I. Kejnovská, K. Bednářová, D. Renčiuk, J. Kypr, Circular Dichroism Spectroscopy of DNA: From Duplexes to Quadruplexes, Chirality 24 (9) (2012) 691–698.

[36] N. Sugimoto, N. Satoh, K. Yasuda, S.-I. Nakano, Stabilization Factors Affecting Duplex Formation of Peptide Nucleic Acid with DNA, Biochemistry 40 (29) (2001) 8444–8451.

[37] M. Massaro, S. Riela, S. Guernelli, F. Parisi, G. Lazzara, A. Baschieri, L. Valgimigli, R. Amorati, A synergic nanoantioxidant based on covalently modified halloysite–trolox nanotubes with intra-lumen loaded quercetin, J. Mater. Chem. B 4 (13) (2016) 2229–2241.

[38] S. Volpi, U. Cancelli, M. Neri, R. Corradini, Multifunctional Delivery Systems for Peptide Nucleic Acids, Pharmaceuticals 14 (1) (2021) 14.

[39] M. Massaro, G. Barone, G. Biddeci, G. Cavallaro, F. Di Blasi, G. Lazzara, G. Nicotra, C. Spinella, G. Spinelli, S. Riela, Halloysite nanotubes-carbon dots hybrids multifunctional nanocarrier with positive cell target ability as a potential non-viral vector for oral gene therapy, J. Colloid Interface Sci. 552 (2019) 236–246.

[40] X. Mo, F. Wu, B. Yu, W. Wang, X. Cai, Folate-PG modified halloysite nanotube for enhancing tumor targeting and anticancer efficacy, Appl. Clay Sci. 193 (2020) 105664.

[41] M.L. Alfieri, M. Massaro, M. d'Ischia, G. D'Errico, N. Gallucci, M. Gruttadauria, M. Licciardi, L.F. Liotta, G. Nicotra, G. Sfuncia, S. Riela, Site-specific halloysite functionalization by polydopamine: A new synthetic route for potential near infrared-activated delivery system, J. Colloid Interface Sci. 606 (2022) 1779–1791.

[42] X. Li, J. Chen, H. Liu, Z. Deng, J. Li, T. Ren, L. Huang, W. Chen, Y. Yang, S. Zhong, β-Cyclodextrin coated and folic acid conjugated magnetic halloysite nanotubes for targeting and isolating of cancer cells, Colloids Surf. B Biointerfaces 181 (2019) 379–388.

[43] R. Brazil, Peptide Nucleic Acids Promise New Therapeutics and Gene Editing Tools, ACS Centr. Sci. 9 (1) (2023) 3–6.